European Journal of Medicinal Chemistry 81 (2014) 35–46

Contents lists available at ScienceDirect

European Journal of Medicinal Chemistry

journal homepage: http://www.elsevier.com/locate/ejmech

Original article

# Molecular basis of the selective binding of MDMA enantiomers to the alpha4beta2 nicotinic receptor subtype: Synthesis, pharmacological evaluation and mechanistic studies

Salomé Llabrés [a,1], Sara García-Ratés [b,1], Edgar Cristóbal-Lecina [c], Antoni Riera [c], José Ignacio Borrell [d], Jorge Camarasa [b], David Pubill [b], F. Javier Luque [a], Elena Escubedo [b,*]

[a] Department of Physical Chemistry and Institut of Biomedicine (IBUB), Faculty of Pharmacy, Campus de l'Alimentació Torribera, University of Barcelona, Avda. Prat de la Riba 171, Santa Coloma de Gramenet, E-08921 Barcelona, Spain
[b] Department of Pharmacology and Therapeutic Chemistry and Institut of Biomedicine (IBUB), Faculty of Pharmacy, University of Barcelona, Nucli Univ. Pedralbes, E-08028 Barcelona, Spain
[c] Institute for Research in Biomedicine (IRB Barcelona), Baldiri i Reixac, 10, 08028 Barcelona, Spain
[d] IQS School of Engineering, Universitat Ramon Llull, Via Augusta 390, E-08017 Barcelona, Spain

*Keywords:*
Alpha4Beta2 nicotinic receptor
MDMA
Enantioselective binding
Receptor up-regulation
Molecular modelling
Stereoselective synthesis

A B S T R A C T

The α4β2 nicotinic acetylcholine receptor (nAChR) is a molecular target of 3,4-methylenedioxymethamphetamine (MDMA), a synthetic drug also known as ecstasy, and it modulates the MDMA-mediated reinforcing properties. However, the enantioselective preference of the α4β2 nAChR subtype still remains unknown. Since the two enantiomers exhibit different pharmacological profiles and stereoselective metabolism, the aim of this study is to assess a possible difference in the interaction of the MDMA enantiomers with this nAChR subtype. To this end, we report a novel simple, yet highly efficient enantioselective synthesis of the MDMA enantiomers, in which the key step is the diastereoselective reduction of imides derived from optically pure *tert*-butylsulfinamide. The enantioselective binding to the receptor is examined using [$^3$H]epibatidine in a radioligand assay. Even though the two enantiomers induced a concentration-dependent binding displacement, (*S*)-MDMA has an inhibition constant 13-fold higher than (*R*)-MDMA, which shows a Hill's coefficient not significantly different from unity, implying a competitive interaction. Furthermore, when NGF-differentiated PC12 cells were pretreated with the compounds, a significant increase in binding of [$^3$H]epibatidine was found for (*R*)-MDMA, indicating up-regulation of heteromeric nAChR in the cell surface. Finally, docking and molecular dynamics studies have been used to identify the binding mode of the two enantiomers, which provides a structural basis to justify the differences in affinity from the differential interactions played by the substituents at the stereogenic centre of MDMA. The results provide a basis to explore the distinct psychostimulant profiles of the MDMA enantiomers mediated by the α4β2 nAChR subtype.



## 1. Introduction

3,4-Methylenedioxymethamphetamine (MDMA; Scheme 1), also known as ecstasy, is a synthetic drug widely abused in the United States and Europe, where it is taken in a recreational context due to its stimulant and hallucinogenic properties. Amphetamines produce a dose-dependent increase of locomotor activity in rodents [1], which reflects an increase of dopamine (DA) transmission in the nucleus accumbens [2]. Activation of nicotinic acetylcholine receptors (nAChRs) is a common event in the pathway used by several addictive drugs to stimulate the mesolimbic DA system, which is a relevant component of the brain stimulation reward pathway [3,4]. Thus, in rats systemic nicotine or alcohol administration elevates extracellular DA levels in the nucleus accumbens, an effect that requires stimulation of nAChRs in this area as well as in the ventral tegmental one, in which the mesolimbic dopaminergic cell bodies are located [5–7].

*Abbreviations:* AP, alternative pose; BP, best pose; CNS, central nervous system; DA, dopamine; MD, molecular dynamics; MDMA, N-3,4-methylenedioxymethamphetamine; nAChR, nicotinic acetylcholine receptor; QM/MM, quantum mechanical/molecular mechanical; SIE, Solvated interaction energy.

* Corresponding author.
*E-mail address:* eescubedo@ub.edu (E. Escubedo).

[1] These authors have contributed equally to this work.

http://dx.doi.org/10.1016/j.ejmech.2014.04.044
0223-5234/

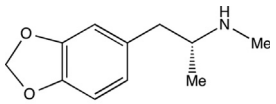


(*R*)-MDMA

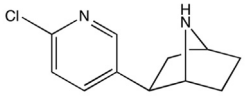


Epibatidine

**Scheme 1.** Molecular structure of epibatidine and (*R*)-MDMA.

The heteromeric α4β2 nAChR subtype, which is involved in regulating the nicotine dependence [8], is strongly associated with DA release in the nucleus accumbens [9] and with drug-seeking behaviour [10,11]. Therefore, it is generally assumed that the α4β2 nAChR subtype plays a major role in reinforcing the effects of nicotine and has been recognized as a major target in addictive pathologies. This is reflected in the hypothesis that the main addictive drugs with psychostimulant properties share the capacity to interact with α4β2 receptors [12,13] In this regard, the α4β2 nAChR subtype can also explain the mechanism of other reinforcing substances. A particular feature of nAChR is that chronic exposure to nicotinic ligands induces a higher level of epibatidine (Scheme 1) binding to β2-containing nAChRs, leading to a functional up-regulation [14–16] that should enhance the addictive effects of these compounds [8]. This phenomenon is independent of de novo protein synthesis. Vallejo et al. [17] demonstrated that α4β2-subtype receptors exist in two interconvertible states, with high and with low affinities for nicotine, respectively, and that chronic exposure to a nAChR ligand stabilizes a larger fraction of receptors in the high-affinity state at the membrane surface. Other authors [18,19] suggest a chaperone- maturation enhancing effect of nicotine on immature receptors inhibiting its degradation. This is not related to the efficacy of the ligand in activating the receptor but to its affinity.

We have demonstrated that nAChRs are a pharmacological target for MDMA and mediate some actions of this drug of abuse [20,21] including analgesia or locomotor activity [22], tumour necrosis factor alpha suppression [23] and neurotoxicity [24–26]. Recently, Ciudad-Roberts et al. [27] established that the α4β2 nAChR subtype modulates MDMA-mediated reinforcing properties. Previous studies [20,28] had also shown that MDMA has affinity for α4β2 nAChR and induced their up-regulation in PC12 cells following a similar mechanism than that of nicotine. Lately it was reported that rat exposure to nicotine or MDMA each induced significant increases in [$^3$H]epibatidine binding (about 30 and 35%, respectively) with respect to saline-treated rats, and that this effect was significantly potentiated (up to 72%) when the two drugs were associated [21]. Consequently, knowledge of the interaction of MDMA with nAChRs is valuable to understand the role of this receptor in both nicotine and psychostimulant addictions.

MDMA contains a stereogenic centre at the carbon α to the amine (Scheme 1). Even though it is consumed as a racemate, the two enantiomers exhibit different pharmacological profiles and stereoselective metabolism [29,30]. Thus, in vitro models have revealed that (S)-MDMA is more active than (R)-MDMA on the central nervous system (CNS) [31–34]. On the other hand, MDMA is known to undergo extensive hepatic metabolism, leading to the formation of highly redox-active metabolites that have been implicated in MDMA-induced hepato-, neuro-, nephron- and cardiotoxicity [35,36]. However, these effects are sensitive to the enantiomeric form of MDMA. For instance, (*R*)-MDMA primarily contributes to the depletion of the hepatic glutathione induced by the racemic mixture [37]. Moreover, studies in animal models revealed that (*S*)-MDMA rather than (*R*)-MDMA contributes to the serotonergic injury and astroglial and microglial activation associated with MDMA consumption [38,39]. Finally, *rac*-MDMA exerts simultaneous effects, reducing L-DOPA-induced dyskinesia and extending its antiparkinsonian benefits (ON-time) by 5-$HT_{2A}$ antagonism and serotonin transporter selective inhibition, which arise from its *R* and *S* enantiomers, respectively [40].

The aim of this study is to characterize for the first time the interaction of the two enantiomeric forms of MDMA upon binding to the α4β2 nAChR subtype, and to explore the molecular basis of the selective binding to this receptor. To this end, we have examined a novel and efficient strategy for the synthesis of both enantiomers of MDMA based on the diastereomeric reduction of the imides derived from optically pure *tert*-butylsulfinamide. Afterwards, we have evaluated the experimental affinity of both enantiomers for the α4β2 nAChR using radioligand binding assays. Attention has also been paid to the differential effects of the two enantiomers in triggering the α4β2 nAChR up-regulation. Finally, molecular modelling and computational techniques have been used to study the interaction with the α4β2 nAChR subtype and to identify the molecular determinants responsible of the different affinity of the enantiomeric forms of MDMA.

## 2. Results and discussion

### 2.1. Synthesis of MDMA enantiomers

Several enantioselective syntheses of amphetamines have been reported [41–45]. The first stereoselective synthesis of MDMA was based on the hydrogenation of imines derived from 1-phenylethylamine as a chiral auxiliary [41]. The same quiral auxiliary was used by Pizarro et al. in the preparation of enantiomerically enriched HMMA (4-hydroxy-3-methoxymethamphetamine) and HHMA (3,4-dihydroxymethamphetamine) [42]. An enzymatic methodology was reported for the preparation of chiral cyanohydrins that were transformed into 3,4-methylenedioxy amphetamines [43]. Wagner et al. reported a stereospecific synthesis of amphetamines, although it was not applied to MDMA [44]. Recently, Huot et al. published another synthesis of MDMA enantiomers by enantiospecific ring opening of aziridines with a Grignard reagent, even though the experimental details have not been described [40]. These synthetic approaches are not practical since they involve either low diastereoselectivities, costly preparation of the starting ketones or lack of experimental procedures. Therefore, we have developed a new and efficient synthesis of both enantiomers of MDMA based on the diastereomeric reduction of the imides derived from optically pure *tert*-butylsulfinamide.

Our synthesis started from commercially available 3,4-dibenzyloxybenzaldehyde (**1**), which was transformed into the methyl ketone **3** by condensation with nitroethane followed by reduction with Fe/HCl (Scheme 2). The corresponding imine, formed by treatment of ketone **3** with (*R*)-(+)-*tert*-butylsulfinamide and $Ti(OEt)_4$ was reduced *in situ* with $NaBH_4$ at room temperature to afford the two diastereomeric sulfinamides **4** in excellent yield but with moderate (3:1) diastereomeric ratio. Gratifyingly, the diastereoselectivity rose to 14:1 by lowering the temperature to −20 °C in the reduction step. The major isomer was easily purified by crystallization from hexane affording diastereomerically pure **(*R*,*R*$_S$)-4a** as a white solid (Scheme 2).

Methylation of sulfonamide **(*R*,*R*$_S$)-4a** was carried out uneventfully with NaH and MeI in DMF at room temperature to give **(*R*,*R*$_S$)-5a** in 90% yield. However, we were unable to cleave the benzyloxy groups by catalytic hydrogenation (Pd/C) even at high

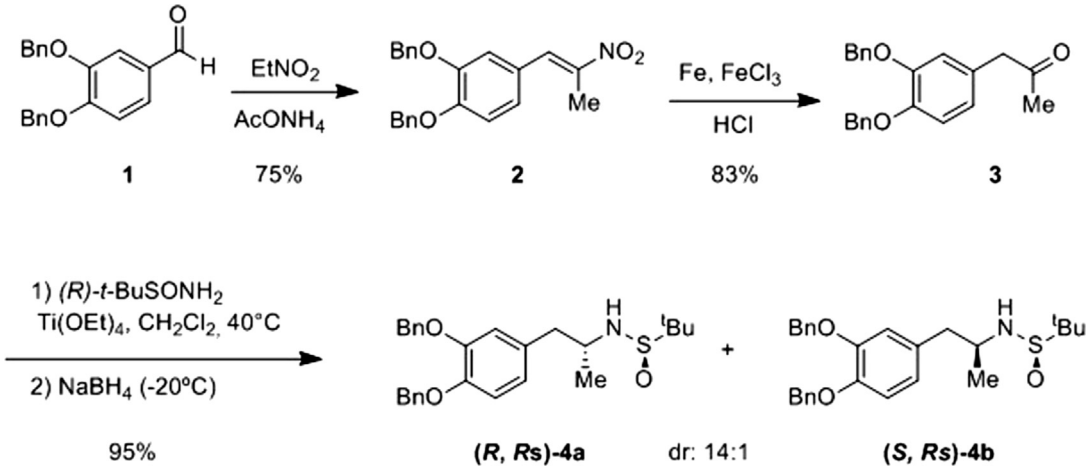


**Scheme 2.** Diastereoselective synthesis of sulfinamides **4**.

hydrogen pressures (50 bar) and/or temperatures (50 °C). We hypothesized that sulphur byproducts derived from sulfinimides hampered the reaction poisoning the catalyst (Scheme 3). Alternatively, derivatization of **(*R*,*R*$_S$)-4a** as ethyl carbamate was unsuccessful since this sulfonamide is a very weak nucleophile. Therefore, we envisaged the hydrolysis of **(*R*,*R*$_S$)-4a** to the primary amine. Reductive cleavage of N–S bond was easily performed with 4 M MeOH/HCl in dioxane affording amine **(*R*)-6a** in 94% yield. Formation of the carbamate of the primary amine **(*R*)-7a** was carried out with $ClCO_2Et$, $Et_3N$ in DMF. This compound was highly crystalline and allowed to confirm its high optical purity (99% ee by chiral HPLC). Cleavage of the dibenzyloxy group in **(*R*)-7a** could be performed by hydrogenolysis and the resulting diphenol was cyclized with bromochloromethane and cesium carbonate as described by Pizarro et al. [42]. Finally, reduction with lithium aluminium hydride in THF yielded the desired compound **(*R*)-10a (MDMA)** in 85% yield, which was isolated as a hydrochloride. The enantiomeric purity of the final product was checked by chiral HPLC of the corresponding N-Boc derivative, being 99% ee, as expected. Since both enantiomers of *tert*-butylsulfinamide are commercially available, the same sequence starting from (*S*)-(−)-*tert*-butylsulfinamide afforded the (*S*)-MDMA enantiomer also in 99% ee.

### 2.2. Experimental binding affinity of MDMA enantiomers

When [$^3$H]epibatidine was used as a radioligand to label the α4β2 nAChR subtype, all the compounds induced a concentration-

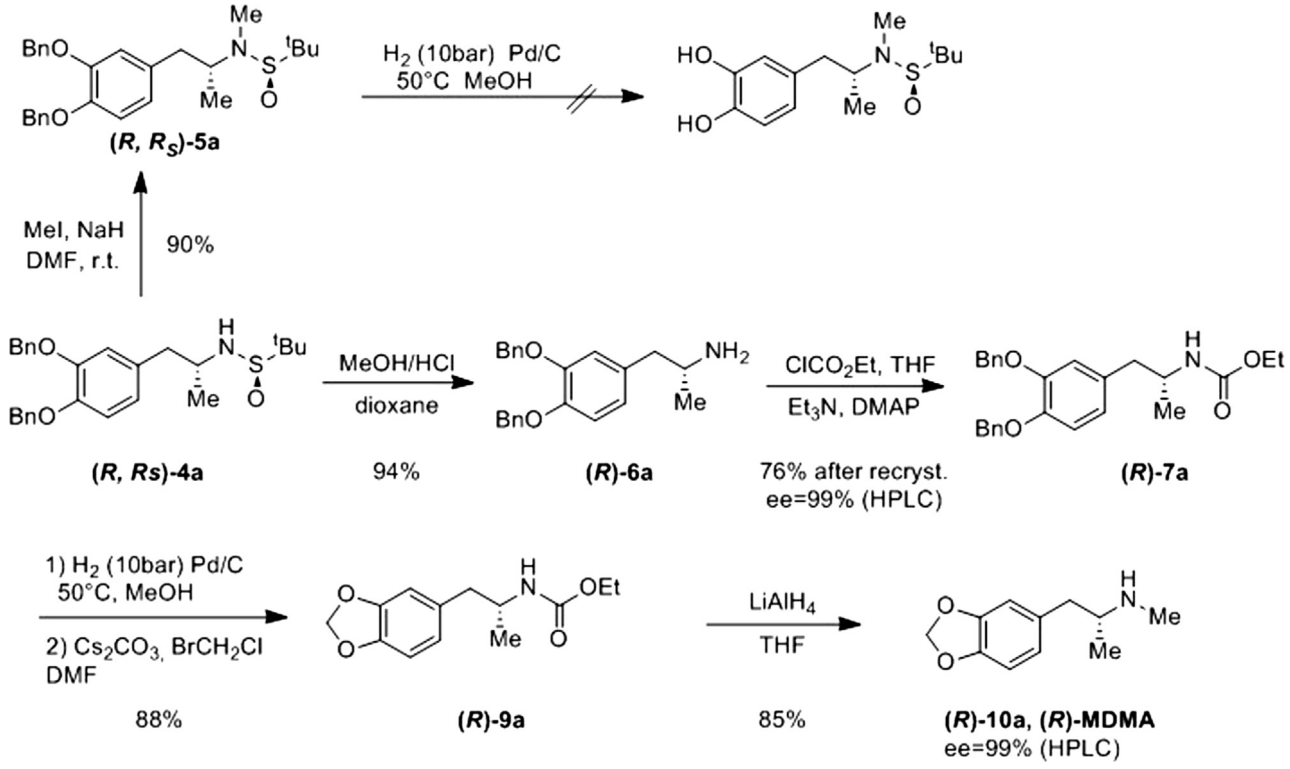


**Scheme 3.** Synthesis of (*R*)-MDMA from diastereomerically pure sulfinamide **4a**.

dependent binding displacement, with $IC_{50}$ values in the micromolar range (see Fig. 1 and Table 1), indicating that they can directly interact with the nicotinic receptor. The affinity of (*R*)-MDMA for the [$^3$H]epibatidine binding site was higher than (*S*)-MDMA, as noted in the 13-fold ratio between the inhibition constants ($K_i$) determined for both enantiomers, respectively (see Table 1). The $K_i$ value of (*R*)-MDMA is in the submicromolar range ($K_i$ = 0.63), which thus compares with the low micromolar concentrations found in the brain after administration of this drug [45,46]. In fact, the binding constant for this heteromeric receptor is lower than the $K_i$ value determined for the serotonin transporter, which is its main physiological target (24.5 μM) [40].

The Hill coefficients resulting from the analysis of competition data of (*R*)-MDMA or *rac*-MDMA *versus* [$^3$H]epibatidine were not significantly different from unity, pointing to a competitive displacement. In contrast, the Hill's coefficient for (*S*)-MDMA was significantly less than unity, suggesting a more complex interaction.

### 2.3. Up-regulation of heteromeric nAChR by MDMA enantiomers

Once established the affinity constants, we tested whether these compounds had any effect on α4β2 nAChR up-regulation. When NGF-differentiated PC12 cells were pretreated with (*R*)-MDMA, (*S*)-MDMA or the racemic mixture for 24 h, at a concentration of 100 μM, a significant increase in binding of [$^3$H]epibatidine was found for (*R*)-MDMA and *rac*-MDMA, indicating up-regulation of heteromeric nAChR. It is known that this up-regulation is independent of de novo protein synthesis [47] but it is consistent with a higher ratio of the high-affinity component of [$^3$H]epibatidine binding [17], as suggested by previous studies on chronic exposure to nicotine [28]. This effect was significantly higher for (*R*)-MDMA than for the racemic mixture (see Fig. 2). (*S*)-MDMA did not significantly modify the nAChR population. These results support the direct interaction with nAChR reported above and corroborates the higher affinity of (*R*)-MDMA compared with (*S*)-MDMA.

### 2.4. Binding mode of MDMA

Previous studies have indicated that the nicotinic binding site is located at the centre of the extracellular domain of the receptor and lies at the interface between α and β subunits, which are known as the principal (P) and complementary (C) components, respectively [48–50]. Several residue stretches referred to as loops A, B and C in the α subunit, and D, E and F in the β subunit shape the binding site (in the following the symbols "α" and "β" will be used before the residue to indicate the subunit it belongs to, and the numbering refers to the α4 and β2 subunits in rat). Conserved residues at the binding site are the aromatic amino acids αTyr128 (loop A), αTrp184 and αTyr186 (loop B), αTyr225 and αTyr232 (loop C) and βTrp81 (loop D). Residues βVal135, βPhe143 and βLeu145 shape the top of the binding site. The bridged cysteine residues in loop C (αCys227 and αCys228) are present only in the α-subunit.

The binding mode of epibatidine, (*R*)-MDMA and (*S*)-MDMA was examined by means of docking calculations with MOE (Chemical Computing Group). The predicted pose of epibatidine nicely reproduced the binding mode observed in the X-ray structure (PDB entries 2BYQ [51] and 3SQ6 [52]), thus giving confidence to the docking protocol. In particular, the binding mode reproduced the cation–pi interaction with the indole ring of αTrp184 (corresponding to Trp147 in 2BYQ) and the hydrogen bond with the carbonyl unit of this residue (see Fig. S1 in Supporting Information). It is worth noting that these interactions are crucial for modulating the affinity of nicotine toward brain and muscle receptor subtypes [53]. Recent studies have also highlighted the relevance of the hydrogen bond with the backbone carbonyl of αTrp184 for the binding of ligands to nAChRs [54].

For (*R*)-MDMA the best pose (denoted BP hereafter; MOE score: −6.7 kcal/mol) obtained in docking calculations nicely matches the structure of epibatidine, as noted in the superposition of the protonated secondary nitrogen atoms and the overlap between the chloropiperidine and methylenedioxybenzene moieties of these compounds (see Fig. 3A). The analysis of the results also showed an alternative pose (designated AP; MOE score: −4.9 kcal/mol) that retains the interaction of the secondary amine with αTrp184, but the methylenedioxybenzene ring adopts a different

**Table 1**
Experimental binding parameters ($IC_{50}$, inhibition constant, $K_i$, and Hill's coefficient, nH) determined for the binding of MDMA to the α4β2 nAChR subtype (SEM: standard error of the mean).

| Ligand | $IC_{50}$ ± SEM (μM) | $K_i$ ± SEM (μM) | nH ± SEM |
|---|---|---|---|
| (*R*)-MDMA | 13.45 ± 2.76 | 0.63 ± 0.16 | 1.02 ± 0.01 |
| (*S*)-MDMA | 172.65 ± 34.58 | 8.21 ± 2.02 | 0.75 ± 0.11[a] |
| *rac*-MDMA | 30.40 ± 6.65 | 1.44 ± 0.54 | 1.03 ± 0.04 |

[a] Significantly different from the value of 1 with $p < 0.001$.

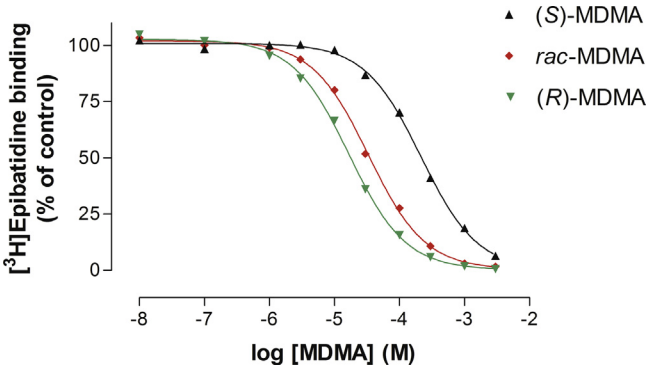


**Fig. 1.** Representative competition curves showing the inhibition of [$^3$H]epibatidine binding by (*R*)-, (*S*)- and (*R*,*S*)-MDMA in membranes from rat brain. Membranes were incubated for 2 h at 4 °C with 2 nM [$^3$H]epibatidine in the absence or the presence of increasing concentrations of MDMA. Inhibition curves were calculated using the nonlinear least squares method and adjusted to a one-site model. Data represent means of duplicates and the experiments were performed three times with similar results.

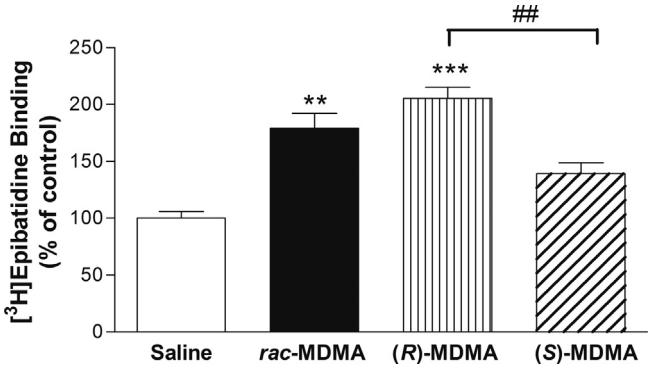


**Fig. 2.** [$^3$H]-Epibatidine binding sites after treatment with (*R*)-, (*S*)- and *rac*-MDMA (100 μM). PC 12 cells were incubated with amphetamine derivatives over 24 h and radioligand binding was performed on intact cells in culture. Data represent the means ± SEM of three separate experiments carried out in triplicates (**$p < 0.01$, ***$p < 0.001$ vs. control cells; ##$p < 0.01$, vs. (*R*)-MDMA).

orientation and fills the region located between the disulfide bridge formed by αCys227-αCys228 and βPhe143 (Fig. 3B).

Docking of (*S*)-MDMA led to similar binding modes as those described for (*R*)-MDMA (see Fig. S2 in Supporting Information). The scores of the two poses (MOE scores of −6.4 and −5.1 kcal/mol for BP and AP solutions, respectively) compare well with those found for (*R*)-MDMA, thus reflecting the similar arrangement of the protonated nitrogen atom and the methylenedioxybenzene unit in the binding site for the equivalent poses of both (*R*)- and (*S*)-MDMA.

### 2.5. Structural basis of the enantioselective binding

MD simulations were run to examine the structural integrity of the two binding modes (BP, AP) found for (*R*)- and (*S*)-MDMA. For (*R*)-MDMA, the simulation started from the BP binding mode (Fig. 3A; designated MD-BP) remained stable along the whole trajectory, as noted in the lack of significant alterations in the positional root-mean square-deviation for the residues that shape the binding site (RMSD ~ 1.9 Å). In contrast, when the AP binding mode (Fig. 3B; denoted MD-AP) was used as the starting structure, a fast rearrangement was observed for the ligand, which adopted the BP binding mode for the rest of the trajectory. The ligand is closely packed in the binding site, forming interactions that are preserved along the whole trajectory (Fig. 4). Thus, the secondary amine nitrogen is located at around 3.3 Å from the indole ring of αTrp184 and maintains the hydrogen bond with the carbonyl group (average distance of 2.9 Å). In addition, the amine nitrogen forms a hydrogen bond with the hydroxyl group of αTyr128, which in turn is hydrogen-bonded to the carbonyl oxygen of αSer183. The methylenedioxybenzene moiety fills a hydrophobic cavity formed by αThr185, βPhe338, βVal135, βPhe143, βTrp144 and βLeu145. The methyl group in the ethylamine chain faces the six-membered rings of αTrp184 and βTrp81 (average distance of 3.7 Å), and the phenol ring of αTyr128 (at 4.0 Å). The ethylene chain forms van der Waals contacts with the disulfide bridge (at around 3.5 Å). Finally, the N-bound methyl interacts with the aromatic ring of αTyr225 and αTyr232 (average distance of 3.9 and 3.5 Å, respectively). Overall, the consistency of the binding modes found in the two independent trajectories supports the binding mode proposed for (*R*)-MDMA.

The trajectories run for the two binding modes of (*S*)-MDMA did not converge to a common binding mode, and the ligand retained the distinct orientation of the methylenedioxybenzene unit. In agreement with docking results, SIE calculations favours the BP binding mode by 0.7 kcal/mol, which reflects the enhanced van der Waals component due to the deeper insertion of the methylenedioxybenzene unit in the binding site (Table S1). Noteworthy, a common feature in the two simulations is the insertion of a water molecule that fills the region between the secondary amine nitrogen and the indole rings of αTrp184 and βTrp81 (Fig. S3). The entrance of the water molecule takes place through the passage shaped by βPhe143 and the disulfide bridge between αCys227 and αCys228 in loop C, which is more flexible in the presence of (*S*)-MDMA (Fig. S4).

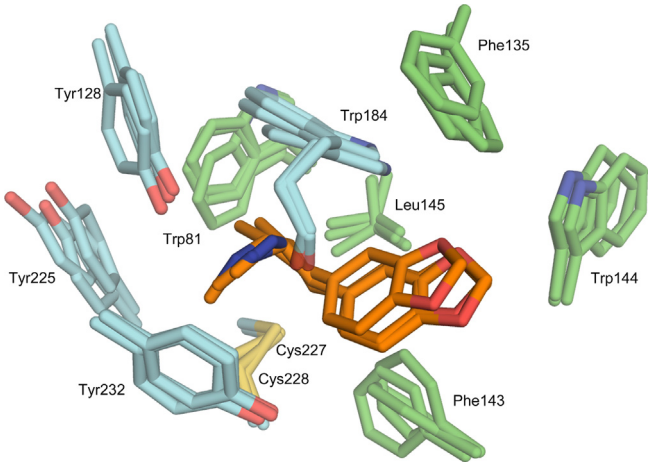


**Fig. 4.** Representation of (*R*)-MDMA in the binding site of the dimeric 3D model of the α4β2 receptor as obtained from MD-BP simulations. Selected residues pertaining to the snapshots collected at 20, 30 and 40 ns of the MD trajectory are shown as blue (α subunit) and green (β subunit) sticks, and the ligand is shown as orange sticks.

The origin of the different behaviour found for the two enantiomeric species can be attributed to the specific interactions formed by the methyl group bound to the stereogenic centre in MDMA. Thus, for (*R*)-MDMA the methyl group is tightly packed against αTrp184 and βTrp81. This position, however, is filled by the water molecule in the complex with (*S*)-MDMA, whereas the methyl group fills a pocket formed by the disulfide bridge and residues αTyr225 and αTyr232 (Fig. 5). Overall, these findings suggest that the specific orientation of the methyl group in (*S*)-MDMA makes the loop C to adopt a less stable fold onto the ligand in the binding pocket, which would exhibit larger fluctuations compared to the binding of (*R*)-MDMA. Since the loop C appears to behave as an 'induced-fit sensor' that can adapt its conformation to the structural features of the ligand bound to the receptor [51], the

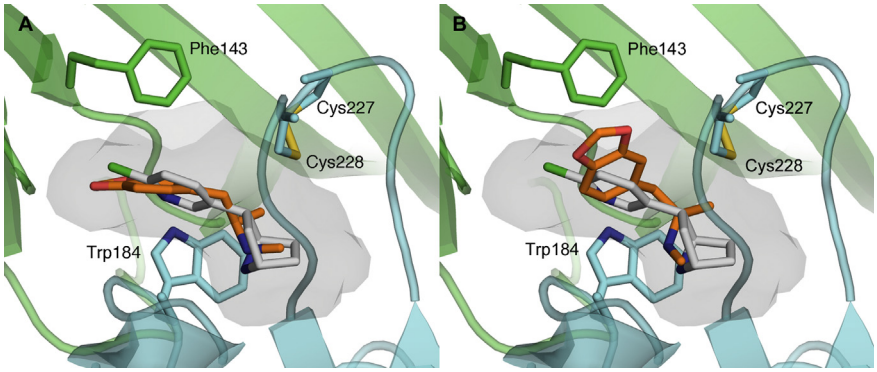


**Fig. 3.** (A) Best pose (BP) of (*R*)-MDMA in the binding site of the dimeric 3D model of the α4β2 receptor. (B) Representation of the alternative pose (AP) characterized by the distinct arrangement of the methylenedioxybenzene ring in the binding pocket. The backbone of the two chains in the dimer is shown in blue (α subunit) and green (β subunit). αTrp184, αCys227 and αCys228 are shown as blue sticks, and βPhe143 as green sticks (R)-MDMA is shown as orange sticks, and epibatidine as white sticks.

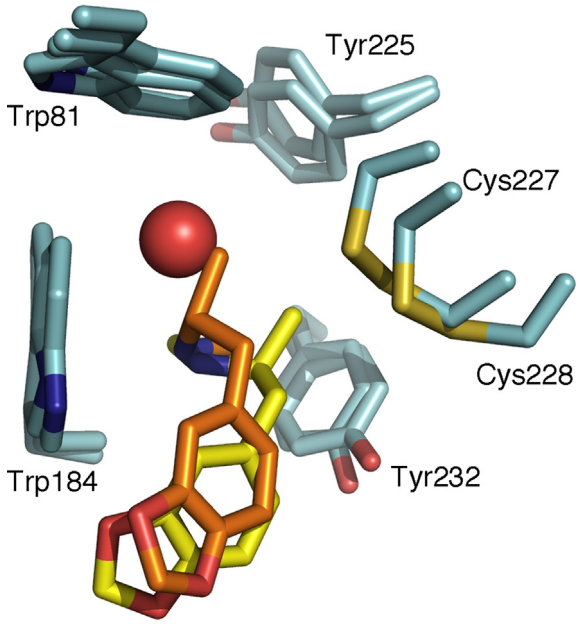


**Fig. 5.** Representation of the closest contacts between the methyl group attached to the ethylamine chain of (*R*)- and (*S*)-MDMA in the receptor binding site. Selected residues pertaining to the snapshot collected at the end of the MD-BP trajectories are shown as sticks. (*R*)- and (*S*)-MDMA are shown as orange and yellow sticks, respectively, and the water molecule that mediates the interaction of the amine nitrogen in (*S*)-MDMA is shown as a red sphere.

largest flexibility observed for (*S*)-MDMA might thus be related to the weaker binding compared to (*R*)-MDMA.

### 2.6. Relative affinities between MDMA enantiomers

To calibrate the reliability of the BP binding mode for both (*R*)- and (*S*)-MDMA, the relative affinity of the two enantiomers was estimated from QM/MM calculations using suitable thermodynamic cycles (Fig. S5). The QM/MM interaction energy between ligand and receptor was found to favour the binding of (*R*)-MDMA by 3.2 kcal/mol with regard to the monohydrated *S* enantiomer. This contribution mainly comes from the van der Waals term, which favours the binding of the *R* enantiomer by 4.6 kcal/mol, suggesting a tighter packing of (*R*)-MDMA in the binding pocket. For the S enantiomer, however, the QM/MM interaction energy must be corrected by the contribution due to the formation of the (*S*)-MDMA-water complex, which was estimated to be −11.4 kcal/mol (at the MP2 level with inclusion of the basis set superposition correction). This contribution, nevertheless, must be corrected by the entropic change due to formation of the monohydrated (*S*)-MDMA, which is estimated to be +8.0 kcal/mol at 298 K, and by the contribution due to the vaporization of the water molecule from liquid, which amounts to +2.1 kcal/mol. By taking into account these corrections, the formation of the (*S*)-MDMA-water complex is estimated to be −1.3 kcal/mol. Accordingly, the binding of (*R*)-MDMA is predicted to be favoured by 1.9 kcal/mol, which compares well with the free energy difference determined from the inhibition constants reported in Table 1 (estimated to be −1.5 kcal/mol).

## 3. Conclusions

Since the two enantiomers of MDMA exhibit different pharmacological profiles and stereoselective metabolism, it is necessary to discern the different mechanism associated with the enantioselective activity of the two enantiomeric forms of this drug, specifically regarding to its interaction with the nicotinic acetylcholine receptor. To this end, this study reports a new and efficient synthesis of both enantiomers of MDMA based on the diastereomeric reduction of the imides derived from optically pure *tert*-butylsulfinamide, which provides a simple, yet practical way of obtaining the two enantiomers of MDMA. The experimental data point out that the α4β2 nicotinic receptor has larger binding affinity for (*R*)-MDMA than for (*S*)-MDMA, as noted by the 13-fold ratio between the inhibitions constants determined in radiolabeled assays. The enantioselective binding of (*R*)-MDMA is consistent with the enhanced up-regulation of the α4β2 nAChR subtype determined in PC12 cultured cells. Therefore, these results indicate that (*R*)-MDMA is the main effector of the effects mediated by this receptor subtype. The molecular modelling studies point out that the two enantiomers adopt a similar arrangement in the binding pocket of the receptor, even though there are significant differences regarding the interactions of the methyl group bound to the stereogenic centre. As a result, the loop C exhibits larger fluctuations in the presence of (*S*)-MDMA, which facilitates the access of water molecules that mediate the binding of the ligand, whereas a tighter interaction is found for (*R*)-MDMA. Overall, this provides a structural basis to pursue the development of novel compounds useful to understand the reinforcing properties of MDMA.

## 4. Experimental

### 4.1. Chemical synthesis

#### 4.1.1. (*E*)-1,2-Dibenzyloxy-4-(2-nitroprop-1-en-1-yl)benzene (**2**)

Into a 250 mL round bottomed flask, 3,4-dibenzyloxybenzaldehyde **1** (7.94 g, 24.95 mmol) and ammonium acetate (1.92 g, 24.95 mmol) were dissolved in nitroethane (120 mL) and the mixture heated at reflux for 17 h. Nitroethane was then removed under reduced pressure. The crude was dissolved in ethyl acetate (25 mL) at 40 °C, cooled to r.t. and precipitated with hexane. The solid was filtered and the procedure repeated with the filtrate. Compound **2** (6.49 g, 75% yield) was obtained as a yellow solid.

$^1$**H NMR** (400 MHz, $CDCl_3$): $\delta$ = 2.30 (s, 3H, $CH_3$), 5.21 (s, 2H, $CH_2$), 5.23 (s, 2H, $CH_2$), 6.96–6.98 (m, 1H, CH), 6.99 (s, 1H, CH), 7.00 (m, 1H, CH), 7.29–7.49 (m, 10H, CH), 7.97 (s, 1H, CH). $^{13}$**C NMR** (100 MHz, $CDCl_3$): $\delta$ = 14.1 ($CH_3$), 71.1 ($CH_2$), 71.6 ($CH_2$), 114.4 (CH), 117.0 (CH), 125.0 (CH), 127.27 (CH), 127.33 (CH), 128.18 (CH), 128.22 (CH), 128.79 (CH), 128.81 (CH), 133.8 (CH), 136.7 (C), 136.9 (C), 146.2 (C), 148.7 (C), 150.9 (C=O) ppm. **IR** (film): $\nu_{max}$: 2923, 2857, 1512, 1308, 1264 $cm^{-1}$. **HRMS** (ESI): calc. for $C_{23}H_{22}O_4N^+$ ($[M + H]^+$): 376.1543; found: 376.1547.

#### 4.1.2. 1-(3,4-bis(benzyloxy)phenyl)propan-2-one (**3**)

In a 3 necked round bottomed flask, nitro compound **2** (1.24 g, 3.31 mmol), Fe powder (1.11 g, 19.9 mmol, 6 equiv) and $FeCl_3$ (0.12 mg, 0.76 mmol) were suspended in ethanol (15 mL). To this mixture water (30 mL) and conc HCl (2 mL) were added and the solution was heated at reflux during 5 h. The reaction was cooled down and the pH adjusted to 8 with 40% $NH_4OH$ solution, filtered through celite and extracted with EtOAc. The organic phase was washed with water, dried with $MgSO_4$ and evaporated to give a brown crude, which was purified by column chromatography ($SiO_2$/hexanes/ethyl acetate) to afford **3** (0.95 g, 83% yield) as brown oil.

$^1$**H NMR** (400 MHz, $CDCl_3$): $\delta$ = 2.07 (s, 3H, $CH_3$), 3.57 (s, 2H, $CH_2$), 5.14 (s, 4H, $CH_2$), 6.72 (dd, $J$ = 8.2 Hz, 1H, CH), 6.78 (d, $J$ = 2.0 Hz, 1H, CH), 6.90 (d, $J$ = 8.0 Hz, 1H, CH), 7.27–7.39 (m, 6H, CH), 7.41–7.44 (m, 2H, CH). $^{13}$**C NMR** (100 MHz, $CDCl_3$): $\delta$ = 29.2 ($CH_3$), 50.6 ($CH_2$), 71.43 ($CH_2$), 71.49 ($CH_2$), 115.4 (CH), 116.5 (CH), 122.6 (CH), 127.4 (CH), 127.5 (CH), 127.6 (CH), 127.90 (CH), 127.93

(CH), 128.6 (CH), 137.3 (C), 137.4 (C), 148.3 (C), 149.1 (C), 206.8 (C=O) ppm. **IR** (film): $\nu_{max}$: 1708, 1512, 1262, 1137 $cm^{-1}$ **HRMS** (ESI): calc. for $C_{23}H_{23}O_3^+$ ($[M + H]^+$): 347.1642; found: 347.1651.

#### 4.1.3. (R,$R_S$)-N-[1-(3,4-Dibenzyloxyphenyl)propan-2-yl]-tert-butylsulfinamide, (***R,R_S*)-4a**

In a 2 necked 250 mL round bottomed flask was dissolved (*R*)-(+)-*tert*-butylsulfinamide (0.49 g, 4.0 mmol, 2 equiv) in anhydrous THF (11 mL). To this solution was added $Ti(OEt)_4$ (4.2 mL, 20.2 mmol, 10 equiv) and **3** (0.7 g, 2.0 mmol) in anhydrous THF (13 mL). The brown solution was heated to reflux and monitored by TLC. After 5 h the reaction was allowed to cool to room temperature. The reaction was then cooled down to −20 °C, $NaBH_4$ (76 mg, 2.0 mmol, 1 equiv) was added and the reaction was stirred 3 h at −20 °C and overnight at room temperature. The solution was then filtered through celite and the solvent evaporated under reduced pressure. The crude showed a 14:1 diastereomeric ratio by NMR. Column chromatography ($SiO_2$, hexane/ethyl acetate) afforded **(*R,R_S*)-4a** (0.80, 95% yield) as a white solid.

**M.p.**: 91.3–92.6 °C **$[\alpha]_D$** −53.6 (*c* 0.7, MeOH). **$^1$H NMR** (400 MHz, $CDCl_3$): $\delta$ = 1.12 (d, *J* = 6.3 Hz, 3H, $CH_3$), 1.15 (s, 9H, $CH_3$), 2.72 (qd, *J* = 6.6, 13.5 Hz, 2H, $CH_2$), 3.19 (d, *J* = 4.5 Hz, 1H, NH), 3.58 (m, 1H, CH), 5.14 (m, 4H, $CH_2$), 6.71 (dd, *J* = 1.9, 8.1 Hz, 1H, CH), 6.82 (d, *J* = 1.9 Hz, 1H, CH), 6.87 (d, *J* = 8.1 Hz, 1H, CH), 7.27–7.39 (m, 6H, CH), 7.41–7.46 (m, 4H, CH) ppm. **$^{13}$C NMR** (100 MHz, $CDCl_3$): $\delta$ = 20.7 ($CH_3$), 22.7 ($CH_3$), 44.2 ($CH_2$), 51.5 (CH), 55.5 (C), 71.48 ($CH_2$), 71.59 ($CH_2$), 115.5 (CH), 116.7 (CH), 112.7 (CH), 127.46 (CH), 127.53 (CH), 127.88 (CH), 127.91(CH), 128.58 (CH), 128.59 (CH), 130.92 (C), 137.4 (C), 137.5 (C), 147.9 (C), 149.1 (C) ppm. **IR** (film): $\nu_{max}$: 3025, 3033, 2969, 1508, 1271 $cm^{-1}$. **HRMS** (ESI): Calc. for $C_{27}H_{33}NO_3SNa^+$ ($[M + Na]^+$): 474.2073; found: 474.2071. Calc for $C_{54}H_{67}N_2O_6S_2^+$ ($[2\ M + H]^+$): 903.4435; found: 903.4424. **EA**. Calc. for $C_{27}H_{33}NO_3S$: C, 71.81: H, 7.37; N, 3.10; S, 7.10. found: C, 71.83; H, 7.45; N, 3.36, S, 7.02.

#### 4.1.4. (S,$S_S$)-N-[1-(3,4-Dibenzyloxyphenyl)propan-2-yl]-tert-butylsulfinamide, (***S,S_S*)-4a**

The procedure described for **(*R,R_S*)-4a,** starting from **3** (2.9 g, 8.36 mmol), $Ti(OEt)_4$ (17.4 mL, 83.7 mmol, 10 equiv) and (*S*)-(-)-*tert*-butylsulfinamide: (2.0 g, 16.8 mmol, 2 equiv), afforded 3.4 g (90% yield) of **(*S,S_S*)-4a. M.p.** 90.1–90.4 °C. **$[\alpha]_D$** −51.0 (*c* 0.7, MeOH). The spectroscopic data were identical to **(*R,R_S*)-4a.**

#### 4.1.5. (R,$R_S$)-N-[1-(3,4-dibenzyloxyphenyl)propan-2-yl]-N-methyl-tert-butylsulfinamide, (***R,R_S*)-5a**

In a 10 mL round bottomed flask, NaH (4 mg, 0.17 mmol, 2 equiv) was suspended in anhydrous DMF (1.5 mL). A solution of **4a** (34 mg, 0.075 mmol) in anhydrous DMF (3.5 mL) was added and the reaction stirred 20 min at room temperature. MeI (28 μL, 0.45 mmol, 6 equiv) was added via syringe and the reaction was monitored by TLC. When the starting material was consumed, water (10 mL) and EtOAc (10 mL) were added. Phases were separated and the organic phase was dried ($MgSO_4$) and evaporated to give a yellow oil. Column chromatography ($SiO_2$, hexanes/ethyl acetate) afforded **(*R,R_S*)-5a** (33 mg, 99% yield) as a yellow oil.

**$^1$H NMR** (400 MHz, $CDCl_3$): $\delta$ = 1.06 (d, *J* = 6.7 Hz, 3H, $CH_3$), 1.14 (s, 9H, $CH_3$), 2.56 (s, 3H, $CH_3$), 2.57 (m, 1H, $CH_2$), 2.88 (dd, *J* = 4.8, 13.3 Hz, 1H, $CH_2$), 3.38 (m, 1H, CH), 5.13 (s, 2H, $CH_2$), 5.16 (s, 2H, $CH_2$), 6.67 (dd, *J* = 2.0, 8.1 Hz, 1H, CH), 6.74 (d, *J* = 2.0 Hz, 1H, CH), 6.86 (d, *J* = 8.2 Hz, 1H, CH) 7.28–7.39 (m, 6H, CH), 7.41–7.46 (m, 4H, CH) ppm. **$^{13}$C NMR** (100 MHz, $CDCl_3$): $\delta$ = 17.6 ($CH_3$), 23.7 ($CH_3$), 26.5 ($CH_3$), 41.1 ($CH_2$), 58.2 (CH), 60.7 (C), 71.6 ($CH_2$), 115.4 (CH), 116.8 (CH), 122.4 (CH), 127.48 (CH), 127.54 (CH), 127.9 (CH), 128.6(CH), 132.5 (C), 137.5 (C), 137.6 (C), 147.8 (C), 149.0 (C) ppm. **IR** (film): $\nu_{max}$: 3436, 2923, 2872, 1508, 1264 $cm^{-1}$ **HRMS** (ESI): calc. for $C_{28}H_{36}NO_3S^+$ ($[M + H]^+$): 466.2410; found: 466.2419.

#### 4.1.6. (R)-1-(3,4-Bis(benzyloxy)phenyl)propan-2-amine, (***R*)-6a**

In a 250 mL round bottomed flask, a solution of **4a** (1.73 g, 3.82 mmol) in MeOH (15 mL) was placed. 4 M HCl in dioxane (15 mL) was added dropwise at room temperature. The reaction was stirred overnight. The solution was extracted with 0.1 M HCl (20 mL × 5). The aqueous phase was treated with 1 M NaOH (20 mL) and extracted with EtOAc (15 mL × 5). The organic phases where dried ($MgSO_4$) and evaporated to afford **(*R*)-6a** (1.25 g, 94% yield) as a colourless oil.

**$[\alpha]_D$** = −4.7 (*c* 0.7, MeOH). **$^1$H NMR** (400 MHz, MeOD): $\delta$ = 1.1 (m, 3H, $CH_3$), 2.70 (dd, *J* = 7.8, 13.7 Hz, 1H, $CH_2$), 2.85 (dd, *J* = 6.2, 13.6 Hz, 1H, $CH_2$), 3.43 (m, 1H, CH), 5.12 (s, 2H, $CH_2$), 5.14 (s, 2H, $CH_2$), 6.78 (dd, *J* = 4.0, 8.1 Hz, 1H, CH), 6.91 (d, *J* = 1.6 Hz, 1H, CH), 7.01 (d, *J* = 8.2 Hz, 1H, CH), 7.26–7.37 (m, 6H, CH), 7.41–7.46 (m, 4H, CH) ppm. **$^{13}$C NMR** (100 MHz, MeOD): $\delta$ = 18.3 ($CH_3$), 41.3 ($CH_2$), 50.3 (CH), 72.4 ($CH_2$), 72.5 ($CH_2$), 116.8 (CH), 117.7 (CH), 123.5 (CH), 128.67 (CH), 128.74 (CH), 128.92 (CH), 128.95 (CH), 129.45 (CH), 129.47(CH), 130.6 (C), 138.69 (C), 138.74 (C), 149.7 (C), 150.4 (C) ppm. **IR** (film): $\nu_{max}$: 3045, 2923, 1508, 1258 $cm^{-1}$. **HRMS (ESI):** Calc. for $C_{23}H_{26}O_2N^+$ ($[M + H]^+$): 348.1958; found: 348.1957. Calc. for $C_{23}H_{25}O_2NNa^+$ ($[M + Na]^+$): 370.1778; found: 370.1778.

#### 4.1.7. (S)-1-(3,4-Bis(benzyloxy)phenyl)propan-2-amine, (***S*)-6a**

The procedure described for **(*R*)-6a** starting from **(*S*)-4a** (1.52 g, 3.36 mmol) and using 4 M HCl in dioxane (15 mL) afforded 0.97 g (83% yield) of **(*S*)-6a. $[\alpha]_D$** = +3.1 (*c* 0.7, MeOH). The spectroscopic data were identical to **(*R*)-6a.**

#### 4.1.8. (R)-Ethyl [1-(3,4-dibenzyloxyphenyl)propan-2-yl]carbamate, (***R*)-7a**

In a 100 mL round bottomed flask **6a** (1.25 g, 3.58 mmol), 4-(dimethylamino)pyridine (DMAP) (4.38 mg, 0.04 mmol, 0.01 equiv) and triethylamine (2 mL, 14.33 mmol, 4 equiv) were solved in THF (25 mL). The stirred solution was cooled to 0 °C and a solution of ethyl chloroformate (0.7 mL, 7.17 mmol, 2 equiv) was slowly added. The mixture was stirred 6 h at room temperature. The residue was dissolved in ether (60 mL) and washed with water (20 mL). The aqueous phase was extracted with diethyl ether (2 × 25 mL) and the combined organic phases were washed with water (10 mL), 1 N HCl (20 mL) and brine (10 mL), dried ($MgSO_4$) and evaporated to obtain a white solid. Crystallization from hot heptane (20 mL) was afforded **(*R*)-7a** (1.14 g, 76% yield) as a white solid. The enantiomeric purity was 99% ee by HPLC.

**M.p.** 102.9–104.6. **$[\alpha]_D$** = −7.2 (*c* = 0.7, MeOH). **$^1$H NMR** (400 MHz, $CDCl_3$): $\delta$ = 1.03 (d, *J* = 6.6 Hz, 3H, $CH_3$), 1.22 (t, *J* = 7.1 Hz, 3H, $CH_3$), 2.57 (dd, *J* = 7.2, 13.5 Hz, 1H, $CH_2$), 2.73 (dd, *J* = 5.0, 13.2 Hz, 1H, $CH_2$), 3.88 (bs, 1H, NH), 4.09 (m, 2H, $CH_2$), 4.43 (bs, 1H, CH), 5.13 (s, 2H, $CH_2$), 5.14 (s, 2H, $CH_2$), 6.68 (dd, *J* = 1.9, 8.1 Hz, 1H, CH), 6.77 (s, 1H, CH), 6.86 (d, *J* = 8.1 Hz, 1H, CH), 7.27–7.39 (m, 6H, CH), 7.41–7.46 (m, 4H, CH) ppm. **$^{13}$C NMR** (100 MHz, $CDCl_3$): $\delta$ = 14.6 ($CH_3$), 20.0 ($CH_3$), 42.2 ($CH_2$), 47.7 (CH), 60.5 ($CH_2$), 71.2 ($CH_2$), 71.3 ($CH_2$), 115.0 (CH), 116.5 (CH), 122.4 (CH), 127.2 (CH), 127.3 (CH), 127.6 (CH), 127.7 (CH), 128.4 (CH), 131.3 (C), 137.2 (C), 137.4 (C), 147.6 (C), 148.6 (C), 155.8 (C=O). **IR** (film): $\nu_{max}$: 3340, 2971, 1682, 1537, 1513 $cm^{-1}$. **HRMS** (ESI): calc. for $C_{26}H_{30}O_4N^+$ ($[M + H]^+$): 420.21693; found: 420.21723. Calc. for $C_{26}H_{29}O_4NNa^+$ ($[M + Na]^+$): 442.19888; found: 442.19913. **Analysis**. Calc. for $C_{26}H_{29}NO_4$: C, 74.84; H, 6.97; N, 3.34; Found: C, 74.71; H, 7.02; N, 3.75. **HPLC:** CHIRALCEL AS, 80% heptane-20% IPA, 0.5 mL/min, $\lambda$ = 254 nm, $t_{(S)}$ = 14.8 min, $t_{(R)}$ = 17.0 min. Optical purity 99% ee.

*4.1.9. (S)-Ethyl [1-(3,4-dibenzyloxyphenyl)propan-2-yl]carbamate, **(S)-7a***

The procedure described for ***(R)*-7a** starting from **(*S*)-6a** (0.97 g, 2.78 mmol) and using DMAP (3.4 mg, 0.03 mmol, 0.01 equiv), $EtN_3$ (1.6 mL, 11.1 mmol, 4 equiv) and ethyl chloroformate (0.53 mL, 5.57 mmol, 2 equiv) afforded 1.02 g (88% yield) of ***(S)*-7a.**

**M.p.** 103.4–104.5 °C. $[\alpha]_D$ = +5.5 ($c$ = 0.7, MeOH). The spectroscopic data were identical to ***(R)*-7a. HPLC:** CHIRALCEL AS, 80% heptane-20% IPA, 0.5 mL/min, $\lambda$ = 254 nm, $t_{(S)}$ = 14.8 min, $t_{(R)}$ = 17.0 min. Optical purity 99% ee.

*4.1.10. (R)-Ethyl [1-(3,4-dihydroxyphenyl)propan-2-yl]carbamate, **(R)-8a***

To a solution **7a** (1.08 g, 2.58 mmol) in methanol (37 mL) was added 10wt % Pd/C (0.03 g, 0.1 equiv). The suspension was hydrogenated at 10 bar of $H_2$ and 65 °C during 15 h. The solution was filtered through celite and evaporated to yield **(*R*)-8a** (615 mg, 99% of yield) as a brown oil.

$[\alpha]_D$ = −14.9 ($c$ = 0.2, MeOH). **$^1$H NMR** (400 MHz, MeOD): $\delta$ = 1.06 (d, $J$ = 6.3 Hz, 3H, $CH_3$), 1.20 (t, $J$ = 7.0 Hz, 3H, $CH_3$), 2.46 (m, 1H, $CH_2$), 2.65 (m, 1H, $CH_2$), 3.74 (m, 1H, CH), 4.02 (m, 2H, $CH_2$), 6.50 (m, 1H, CH), 6.63 (m, 1H, CH), 6.66 (m, 1H, CH) ppm. **$^{13}$C NMR** (100 MHz, MeOD): $\delta$ = 15.0 ($CH_3$), 20.4 ($CH_3$), 43.6 ($CH_2$), 49.7 (CH), 61.5 ($CH_2$), 116.1 (CH), 117.4 (CH), 121.7 (CH), 131.8 (C), 144.8 (C), 146.0 ($CH_2$), 158.5 (C=O) ppm. IR (film): $\nu_{max}$: 3339, 2977, 2929, 1689, 1063 $cm^{-1}$. **HRMS (ESI)**: Calc. for $C_{12}H_{18}O_4N^+$ ($[M + H]^+$): 240.1230; found: 240.1230. Calc. for $C_{12}H_{17}O_4NNa^+$ ($[M + Na]^+$): 262.1050; found: 262.1049.

*4.1.11. (S)-Ethyl [1-(3,4-dihydroxyphenyl)propan-2-yl]carbamate, **(S)-8a***

The procedure described for ***(R)*-8a** starting from **(*S*)-7a** (730 mg, 1.74 mmol) and using Pd/C (18.5 mg, 0.1 equiv) afforded 415 mg (99% yield) of ***(S)*-8a.**

$[\alpha]_D$ = +15.0 ($c$ = 0.2, MeOH). The spectroscopic data were identical to ***(R)*-8a.**

*4.1.12. (R)-Ethyl 1-(benzo[d][1,3]dioxol-5-yl)propan-2-ylcarbamate, **(R)-9a***

To a solution of **(*R*)-8a** (668 mg, 2.79 mmol) and $CsCO_3$ (2.95 g, 8.37 mmol, 3 equiv) in DMF (20 mL) was added $BrCH_2Cl$ (0.3 mL, 4.47 mmol, 1.6 equiv) and the mixture was stirred for 2 h at room temperature. The solution was filtered through celite and evaporated. The residue was then dissolved in ethyl acetate (200 mL) and washed with water (2 × 25 mL) and brine (25 mL). The organic layer was dried ($MgSO_4$) filtered and the solvent was evaporated to afford **(*R*)-9a** (0.69 g, 89% yield) as a white solid.

$[\alpha]_D$ = −11.0 ($c$ = 0.2, MeOH). **$^1$H NMR** (400 MHz, $CDCl_3$): $\delta$ = 1.10 (d, $J$ = 6.6 Hz, 3H, $CH_3$), 1.23 (t, $J$ = 7.1 Hz, 3H, $CH_3$), 2.60 (dd, $J$ = 7.2, 13.5 Hz, 1H, $CH_2$), 2.75 (m, 1H, $CH_2$), 3.90 (m, 1H, CH), 4.09 (m, 2H, $CH_2$), 4.47 (bs, 1H, NH), 5.93 (m, 2H, $CH_2$), 6.62 (dd, $J$ = 1.6, 7.9 Hz, 1H, CH), 6.67 (d, $J$ = 1.5 Hz, 1H, CH), 6.74 (d, $J$ = 8.0 Hz, 1H, CH) ppm. **$^{13}$C NMR** (100 MHz, $CDCl_3$): $\delta$ = 14.8 ($CH_3$), 20.3 ($CH_3$), 42.7($CH_2$), 48.1 (CH), 60.8 ($CH_2$), 101.0 ($CH_2$), 108.3 (CH), 109.9 (CH), 122.5 (CH), 131.9 (C), 146.3 (C), 147.7 (C), 156.0 (C=O) ppm. **IR (film)**: $\nu_{max}$: 3327, 2968, 2923, 1700, 1245 $cm^{-1}$. **HRMS** (ESI): Calc. for $C_{13}H_{18}O_4N^+$ ($[M + H]^+$): 252.12303; found: 252.12332. Calc. for $C_{13}H_{17}O_4NNa^+$ ($[M + Na]^+$): 274.1050; found: 274.1053.

*4.1.13. (S)-Ethyl 1-(benzo[d][1,3]dioxol-5-yl)propan-2-ylcarbamate, **(S)-9a***

The procedure described for ***(R)*-9a** starting from **(*S*)-8a** (458 mg, 1.91 mmol) and using $Cs_2CO_3$ (2.03 g, 5.75 mmol, 3 equiv) in DMF (12 mL). and $BrCH_2Cl$: (0.2 mL, 3.06 mmol, 1.6 equiv) afforded 460 mg (95% yield) of ***(S)*-9a.**

$[\alpha]_D$ = +11.4 ($c$ = 0.2, MeOH). The spectroscopic data were identical to ***(R)*-9a.**

*4.1.14. (R)-1-(benzo[d][1,3]dioxol-5-yl)-N-methylpropan-2-amine, **(R)-10a**, (R)-MDMA*

A solution of **(*R*)-9a** (106 mg, 0.42 mmol) in anh THF (5 mL) was added dropwise to a suspension of $LiAlH_4$ (0.048 g, 1.26 mmol, 3 equiv) in anh THF (3 mL). The mixture was refluxed with stirring for 4 h and then allowed to cool to room temperature. The excess $LiAlH_4$ was destroyed by slow addition of water at 0 °C. Ethyl acetate was added, extracted with $NH_4Cl$ (5 mL) and NaCl (5 mL). The organic layers were dried over anhydrous $MgSO_4$, filtered and the solvent was removed under reduced pressure affording **(*R*)-10a** (70 mg, 0.36 mmol) in 85% of yield as a colourless oil. This compound was then dissolved in anhydrous diethyl ether (4 mL) and 2 M HCl in diethyl ether was added dropwise, yielding the corresponding hydrochloride **HCl (*R*)-10a** as a white solid.

$[\alpha]_D$ = −12.4 ($c$ = 0.6, $H_2O$). **$^1$H NMR** (400 MHz, $D_2O$): $\delta$ = 1.29 (d, $J$ = 6.6 Hz, 3H, $CH_3$), 2.71 (s, 3H, $CH_3$), 2.86 (dd, $J$ = 7.6, 13.8 Hz, 1H, $CH_2$), 2.99 (dd, $J$ = 6.5, 14.0 Hz, 1H, $CH_2$), 3.50 (m, 1H, CH), 5.99 (s, 2H, $CH_2$), 6.80 (dd, $J$ = 1.7, 8.0 Hz, 1H, CH), 6.86 (d, $J$ = 1.3 Hz, 1H, CH), 6.91 (d, $J$ = 7.9 Hz, 1H, CH) ppm. **$^{13}$C NMR** (100 MHz, $D_2O$): $\delta$ = 14.7 ($CH_3$), 29.9 ($CH_3$), 38.4 ($CH_2$), 56.4 ($CH_2$), 101.0 ($CH_2$), 108.6 (CH), 109.6 (CH), 122.7 (CH), 129.4 (C), 146.2 (C), 147.4 (C). IR (film): $\nu_{max}$: 2955, 2731, 2469, 1482, 1264.8 $cm^{-1}$. **HRMS** (ESI): Calc. for $C_{11}H_{16}O_2N^+$ ($[M + H]^+$): 194.1175; found: 194.1177. **HPLC** (on the N-Boc-derivative): CHIRALPAK ADH, 98% heptane, 2% IPA, 0.5 mL/min, $\lambda$ = 210 nm, $t_{(S)}$ = 21.4 min, $t_{(R)}$ = 23.9 min. Optical purity: 99% ee.

*4.1.15. (S)-1-(benzo[d][1,3]dioxol-5-yl)-N-methylpropan-2-amine, **(S)-10a**, (S)-MDMA*

The procedure described for ***(R)*-10a** starting from **(*S*)-9a** (67 mg, 0.27 mmol) and using $LiAlH_4$ (0.030 g, 0.79 mmol) afforded 41 mg (79% yield) of **HCl·*(S)*-10a.**

$[\alpha]_D$ = +14.2 ($c$ = 0.6, $H_2O$). The spectroscopic data were identical to **HCl·*(R)*-10a.**

### 4.2. PC12 cell cultures

The culture was routinely plated in 92 mm dishes (Nunc) coated with collagen and maintained in Dulbecco's modified Eagle's medium (DMEM) supplemented with heat-inactivated 5% foetal bovine serum, 10% horse serum, 10 mM HEPES, 2 mM glutamine, 25 UI/ml penicillin and 25 μg/ml streptomycin. Cells were cultured to semi-confluency in a humidified 5%$CO_2$ atmosphere at 37 °C and medium was changed every 2–3 days. For splitting, cells were dislodged from the dish using a pipette with medium, with a portion of these replated onto new culture dishes. Cells were used between passages 12 and 18.

To ensure their proper differentiation, cells were mechanically dislodged and seeded (200 × $10^3$ cells per well) onto collagen-coated 24-well plates (Nunc) in medium containing 50 ng/ml nerve growth factor (NGF, Upstate Biotechnology, Lake Placid, NY), 1% horse serum, 10 mM HEPES and 2% glutamine in DMEM. Under these conditions, the cells developed a neuronal phenotype with neurite outgrowth that was already apparent 24 h after seeding. As the expression of nAChR varies during the differentiation period, we always used the cells at day 4 of differentiation [55].

### 4.3. Brain membrane preparations

Binding assays were performed using cortical rat brain tissue. Experimental protocols regarding the use of animals in this study were approved by the Animal Ethics Committee of the University of Barcelona under the supervision of the Autonomous Government

of Catalonia, and in accordance with guidelines of the European Communities Council (86/609/ECC). Efforts were made to minimize suffering and reduce the number of animals used.

Male Sprague–Dawley rats were killed by cervical dislocation (under isoflurane anaesthesia). Immediately after sacrifice, they were decapitated and the brains rapidly removed from the skull. The cerebellum was quickly dissected out and discarded, and the rest of brain frozen on dry ice and stored at −80 °C until later use. When required, brains were thawed, pooled and homogenized at 4 °C in 10 volumes of buffer consisting of 5 mM Tris–HCl, 320 mM sucrose and protease inhibitors (aprotinin 4.5 μg/μl, 0.1 mM PMSF and 1 mM sodium orthovanadate), pH 7.4 using a Polytron homogenizer. The homogenates were centrifuged at 15,000 × g for 30 min at 4 °C. The pellets were resuspended in fresh buffer and incubated at 37 °C for 10 min to remove endogenous neurotransmitters. The protein samples were subsequently re-centrifuged and washed two additional times. The final pellets (crude membrane preparations) were resuspended in 50 mM Tris–HCl buffer plus protease inhibitors and stored at −80 °C until later use in radioligand binding experiments. Protein concentration was determined using the Bio-Rad Protein Reagent (Bio-Rad Labs. Inc., Hercules, CA, USA), according to the manufacturer's specifications.

### 4.4. [$^3$H]Epibatidine binding

Competition [$^3$H]epibatidine binding experiments were carried out using the membrane preparations described above. They were performed in glass tubes containing 1 nM [$^3$H]epibatidine (55.5 Ci/mmol), the competing drugs ((*R*)-, (*S*)- and *rac*-MDMA) at increasing concentrations and 200 μg of brain membranes. The incubation buffer consisted of 50 mM Tris–HCl plus protease inhibitors and incubation was carried out for 3 h at 25 °C. Non-specific binding was determined in the presence of 300 μM nicotine. Binding was terminated by rapid filtration under vacuum.

$IC_{50}$ values and Hill coefficients were determined fitting the data to the Hill's equation using nonlinear regression analysis. The inhibition constants ($K_i$) were calculated from the Cheng–Prusoff equation $K_i = IC_{50}/(1 + (L/K_d))$ [56], where $L$ (1 nM) is the total radioligand concentration and $K_d$ is the dissociation constant of the radioligand in rat brain (estimated to be 50 pM [57]).

To measure variations on the surface receptors in PC 12 cells, cells were pretreated for 24 h with either culture medium (control) or 100 μM (*R*)-, (*S*)- or (R,S)-MDMA. Then, a protocol similar to that described for [$^3$H]epibatidine was used with the difference that cells were incubated with 2 nM [$^3$H]epibatidine (55.5 Ci/mmol, Perkin Elmer, Boston, MA) for 90 min at 37 °C and non-specific binding was determined in the presence of 300 μM nicotine. After incubation, the cells were mechanically dislodged and filtered through vacuum. The wells were washed 3 times with ice-cold buffer and the filter was finally washed with 4 mL of it.

In all binding experiments, the radioactivity retained on the filters was counted by liquid scintillation spectrometry. Specific binding was defined as the difference between the radioactivity measured in the absence (total binding) and in the presence (non-specific binding) of an excess of unlabelled ligand. Different determinations were performed in duplicates or triplicates for each experiment with every experiment repeated at least three times with similar results.

### 4.5. Molecular modelling studies: system setup and docking

To address the binding of MDMA to the α4β2 receptor, the homology model of the extracellular domains of the neuronal rat $(\alpha4)_2(\beta2)_3$ nAChR subtype constructed by Le Novère et al. was used (PDB ID: 1OLE) [49]. The 3D model was refined with the software MOE 2008.10. The stereochemical properties were verified and the Ramachandran's φ-ψ dihedral plot of residues showed that the backbone torsion angles tend to cluster in favourable regions (only 2.1% of residues were found in generously allowed regions or disallowed ones), thus supporting the structural model of the receptor. The few residues that were found in certain disallowed regions were supervised and manually corrected. Disulfide bonds were created between residues Cys167-Cys177 and Cys227-Cys228 of subunit α4 and between Cys154-Cys168 of subunit β2.

Docking studies were performed for the agonist epibatidine (*exo*-(+)-1*R*,2*R*,4*S*) and for the two enantiomeric forms of MDMA, which were modelled in their protonated form. Ligands were minimized using the force field MMFF94x. Docking was carried out with Molecular Operating Environment (MOE) 2008.10. (Chemical Computing Group). For all cases 30 runs per ligand were performed. Epibatidine was used as reference to obtain the best docking parameters. The binding site was defined as the box centred in the aromatic moieties of the binding pocket and extended up to around 20 × 22 × 27 Å. To explore for alternative binding sites, a blind docking was also carried out. To this end, the box included all the protein.

### 4.6. Molecular modelling studies: molecular dynamics simulations

The structural integrity of the binding mode was further explored by means of MD simulations performed for the complexes between (*R*)-MDMA and (*S*)-MDMA with the receptor. Due to the huge size of the whole receptor, simulations were performed for a simplified model consisting of the dimeric model containing adjacent α4 and β2 subunits, as derived from the whole 3D model of the pentameric receptor, thus containing the binding site at the dimer interface.

Simulations were run using the PMEMD module of the Amber software package [58]. The parm99SB parameters [59] were used for the protein and the gaff force field [60] was used to assign parameters to the ligands. The charge distribution of the ligands was refined using RESP charges [61] fitted to the B3LYP/6-31G(d) electrostatic potential obtained with Gaussian03 [62]. The system was neutralized and immersed in an octahedral box (12 Å) of TIP3P water molecules [63]. Each simulation system thus contained the protein-ligand complex, $Na^+$ cations and around 18,000 water molecules, leading to around 78,500 atoms.

Starting from the minimized docking positions, a series of 40 ns MD simulations were run for each protein-ligand complex. For each simulated system, a geometry optimization was conducted on two steps. First, the water molecules and counterions were refined though 3000 steps of steepest descent algorithm followed by 1000 steps of conjugate gradient. Last, the whole system was optimized using 3000 steps of steepest descent and 1000 steps of conjugate gradient. Thermalization of the system was performed in the NVT ensemble during five steps of 50 ps, using a time step of 1fs and increasing the temperature from 50 to 298 K. Concomitantly, the inhibitor and the residues that define the binding site were restrained during thermalization using a variable restraint force. Thus, a force constant of 25 kcal $mol^{-1}$ $Å^{-2}$ was used in the first stage of warming up, and was subsequently decreased by increments of 5 kcal $mol^{-1}$ $Å^{-2}$ in the next stages. Following the last stage of thermalization, and prior to the production runs, a short of MD simulation of 0.5 ns in the NPT ensemble was conducted in order to allow the system to achieve a stable density value at 1 atm. Then a 40 ns trajectory was run using SHAKE to all those bonds involving hydrogen atoms, allowing for a timestep of 2 fs, in conjunction with periodic boundary conditions at constant volume and temperature (298 K). Constant temperature was achieved by using the Langevin thermostat whit a collision frequency of 3 $ps^{-1}$,

particle mesh Ewald was used to deal with long range electrostatic interactions, and a cutoff of 9 Å was applied for nonbonded interactions. It is worth noting that through the complete simulation a restraint force of 5 kcal $mol^{-1}$ $Å^{-2}$ was applied to the residues farther than 12 Å from MDMA, which involve interfaces with other subunits or with transmembrane region.

Binding free energies were calculated with the SIETRAJ [64,65] scoring function, which is based in the SIE approach and uses parameters that have been fitted to reproduce binding free energies of a data set of 99 protein-ligand complexes. 500 snapshots sampled during stable parts of the trajectories were examined and treated accordingly with the standard SIE protocol.

### 4.7. QM/MM calculations

In order to estimate the relative affinity between MDMA enantiomers, the thermodynamic cycles shown in Fig. S5 were used. For (*R*)-MDMA, the binding affinity ($\Delta G_{b,aq}$) can be determined from Eq. (1) (see Fig. S5A).

$$\Delta G_{b,aq} = \Delta G_{b,gas} + \Delta G_{sol}(P{\cdot}R) - \Delta G_{sol}(P) - \Delta G_{sol}(R) \quad (1)$$

where $\Delta G_b(P{\cdot}R)_{gas}$ stands for the interaction free energy in the gas phase, and the other terms account for the solvation of the receptor (P), ligand (*R*) and protein–ligand complex (P*R*).

With regard to (*S*)-MDMA, since the interaction is mediated by a water molecule, the binding affinity was decomposed in two steps: (i) the formation of the complex between (*S*)-MDMA and a water molecule (left cycle in Fig. S5B), and (ii) the binding of the monohydrated (*S*)-MDMA to the receptor (right cycle in Fig. S5B). Let us note that the formation of the complex between (*S*)-MDMA in aqueous solution and a water molecule in liquid water does not involve any change in free energy (i.e., $\Delta G_b(S{\cdot}H_2O)_{aq} = 0$). Accordingly, the binding free energy can be determined from Eq. 2.

$$\begin{aligned}\Delta G_{b,aq} = {} & \Delta G_b(P{\cdot}S{\cdot}H_2O)_{aq} = \Delta G_b(S{\cdot}H_2O)_{gas} \\ & + \Delta G_b(P{\cdot}S{\cdot}H_2O)_{gas} + \Delta G_{sol}(P{\cdot}S{\cdot}H_2O) - \Delta G_{sol}(P) \\ & - \Delta G_{sol}(S) - \Delta G_{sol}(H_2O) \end{aligned} \quad (2)$$

The relative affinity between enantiomers can be estimated as noted in Eq (3), which benefits from the cancellation of most of the terms included in Eqs. (1) and (2).

$$\begin{aligned}\Delta\Delta G_{b,aq} = {} & \Delta G_b(S{\cdot}H_2O)_{gas} + \Delta G_b(P{\cdot}S{\cdot}H_2O)_{gas} \\ & + \Delta G_{sol}(P{\cdot}S{\cdot}H_2O) - \Delta G_{sol}(H_2O) \\ & - \Delta G_b(P{\cdot}R)_{gas} - \Delta G_{sol}(P{\cdot}R) \end{aligned} \quad (3)$$

The free energy change due to the formation of the monohydrated (*S*)-MDMA·$H_2O$ in the gas phase ($\Delta G_b(S{\cdot}H_2O)_{gas}$) was determined from quantum mechanical (QM) calculations at the MP2/6-31 + G(d) level, including the basis set superposition error correction [66], and the thermal and entropic contributions estimated by using the harmonic oscillator-rigid rotor model. The contribution due to the formation of the ligand–protein complex ($\Delta G_b(P{\cdot}S{\cdot}H_2O)_{gas}$; $\Delta G_b(P{\cdot}R{\cdot}H_2O)_{gas}$) was determined from hybrid quantum mechanical/molecular mechanical (QM/MM) calculations. To this end, the ligand was treated at the QM level and all the residues located at less than 15 Å of the ligand were treated classically. Accordingly, the electrostatic term accounts for the QM interaction (determined at the MP2/6-31 + G(d) level) of the ligand with the set of point charges of the residues included in the MM region. The van der Waals term was determined using the 6–12 expression as implemented in AMBER. Calculations were performed for a set of 25 snapshots taken evenly along the last 10 ns of the trajectories and averaging the electrostatic and van der Waals components of the individual snapshots. The contribution due to the solvation of the complexes ($\Delta G_{sol}(P{\cdot}S{\cdot}H_2O)$; $\Delta G_{sol}(P{\cdot}R)$) was assumed to cancel. This assumption is motivated by i) the fact that QM/MM calculations were performed using a common set of residues within the sphere (15 Å) that embodies the binding site for the two enantiomers of MDMA, ii) the close structural resemblance of the MM subsystems in the simulations performed for the two enantiomers, indicating the lack of relevant structural rearrangements, and iii) the burial of the water molecule bound to (*S*)-MDMA in the binding cavity. It must be noted, however, that the reliability of this assumption was further supported by MM/PBSA computations performed for the subsystems used in QM/MM calculations. Finally, the solvation free energy of the water molecule was corrected to take into account the contributions due to the changes in standard states in the process of transferring a water molecule from the gas phase (at 1 atm and 298 K) to bulk water [67].

## Conflict of interest

Authors certify that there is no conflict of interest with any financial organization regarding the material discussed in the manuscript.

## Individual contribution to the paper

AR and EC-L designed and performed the synthesis of the MDMA enantiomers. JC, DP and SG-R planned and achieved the pharmacological study, and JIB and SL performed molecular modelling studies. FJL and EE designed the study and wrote the first draft of the manuscript. All authors contributed to and have approved the final manuscript.

## Acknowledgements

This study was supported by grants from the Plan Nacional sobre Drogas (2008/003 and 2010/005), the Spanish Ministerio de Ciencia e Innovación (SAF2010-15948, CTQ2011-23620, SAF2011-27642) and the Generalitat de Catalunya (SGR977, 2009SGR00901, 2009SGR249). SL and EC-L thank the Generalitat de Catalunya and the Ministerio de Ciencia e Innovación for doctoral fellowship. FJL acknowledges the support from ICREA Academia and the Xarxa de Recerca en Química Teòrica I Computacional (XQRTC). Computational facilities from the Center for Scientific and Academic Services of Catalonia (CESCA) are acknowledged.

## Appendix A. Supplementary data

Supplementary data related to this article can be found at http://dx.doi.org/10.1016/j.ejmech.2014.04.044.

## References

[1] J. Izawa, K. Yamanashi, T. Asakura, Y. Misu, Y. Goshima, Differential effects of methamphetamine and cocaine on behavior and extracellular levels of dopamine and 3,4-dihydroxyphenylalanine in the nucleus accumbens of conscious rats, Eur. J. Pharmacol. 549 (2006) 84–90.
[2] T. Ljungberg, U. Ungerstedt, A rapid and simple behavioural screening method for simultaneous assessment of limbic and striatal blocking effects of neuroleptic drugs, Pharmacol. Biochem. Behav. 23 (1985) 479–485.
[3] O. Blomqvist, J.A. Engel, H. Nissbrandt, B. Söderpalm, The mesolimbic dopamine-activating properties of ethanol are antagonized by mecamylamine, Eur. J. Pharmacol. 249 (1993) 207–213.
[4] B. Söderpalm, M. Ericson, P. Olausson, O. Blomqvist, J.A. Engel, Nicotinic mechanisms involved in the dopamine activating and reinforcing properties of ethanol, Behav. Brain Res. 113 (2000) 85–96.

[5] O. Blomqvist, M. Ericson, J.A. Engel, B. Söderpalm, Accumbal dopamine overflow after ethanol: localization of the antagonizing effect of mecamylamine, Eur. J. Pharmacol. 334 (1997) 149–156.
[6] Y. Tizabi, R.L. Copeland Jr., V.A. Louis, R.E. Taylor, Effects of combined systemic alcohol and central nicotine administration into ventral tegmental area on dopamine release in the nucleus accumbens, Alcohol. Clin. Exp. Res. 26 (2002) 394–399.
[7] M. Ericson, A. Molander, E. Löf, J.A. Engel, B. Söderpalm, Ethanol elevates accumbal dopamine levels via indirect activation of ventral tegmental nicotinic acetylcholine receptors, Eur. J. Pharmacol. 467 (2003) 85–93.
[8] A.P. Govind, P. Vezina, W.N. Green, Nicotine-induced upregulation of nicotinic receptors: underlying mechanisms and relevance to nicotine addiction, Biochem. Pharmacol. 78 (2009) 756–765.
[9] N. Champtiaux, C. Gotti, M. Cordero-Erausquin, D.J. David, C. Przybylski, C. Léna, et al., Subunit composition of functional nicotinic receptors in dopaminergic neurons investigated with knock-out mice, J. Neurosci. Off. J. Soc. Neurosci. 23 (2003) 7820–7829.
[10] D.J.K. Balfour, The neuronal pathways mediating the behavioral and addictive properties of nicotine, Handb. Exp. Pharmacol. (2009) 209–233.
[11] B. Le Foll, S.I. Chefer, A.S. Kimes, D. Shumway, E.A. Stein, A.G. Mukhin, et al., Baseline expression of alpha4beta2* nicotinic acetylcholine receptors predicts motivation to self-administer nicotine, Biol. Psychiatry 65 (2009) 714–716.
[12] A. Metaxas, H. Keyworth, J. Yoo, Y. Chen, I. Kitchen, A. Bailey, The stereotypy-inducing and OCD-like effects of chronic "binge" cocaine are modulated by distinct subtypes of nicotinic acetylcholine receptors, Br. J. Pharmacol. 167 (2012) 450–464.
[13] A.R. Tapper, S.L. McKinney, R. Nashmi, J. Schwarz, P. Deshpande, C. Labarca, et al., Nicotine activation of alpha4* receptors: sufficient for reward, tolerance, and sensitization, Science 306 (2004) 1029–1032.
[14] B. Buisson, D. Bertrand, Nicotine addiction: the possible role of functional upregulation, Trends Pharmacol. Sci. 23 (2002) 130–136.
[15] M.J. Marks, J.B. Burch, A.C. Collins, Effects of chronic nicotine infusion on tolerance development and nicotinic receptors, J. Pharmacol. Exp. Ther. 226 (1983) 817–825.
[16] C.M. Flores, S.W. Rogers, L.A. Pabreza, B.B. Wolfe, K.J. Kellar, A subtype of nicotinic cholinergic receptor in rat brain is composed of alpha 4 and beta 2 subunits and is up-regulated by chronic nicotine treatment, Mol. Pharmacol. 41 (1992) 31–37.
[17] Y.F. Vallejo, B. Buisson, D. Bertrand, W.N. Green, Chronic nicotine exposure upregulates nicotinic receptors by a novel mechanism, J. Neurosci. Off. J. Soc. Neurosci. 25 (2005) 5563–5572.
[18] J. Sallette, S. Pons, A. Devillers-Thiery, M. Soudant, L. Prado de Carvalho, J.-P. Changeux, et al., Nicotine upregulates its own receptors through enhanced intracellular maturation, Neuron 46 (2005) 595–607.
[19] R. Srinivasan, R. Pantoja, F.J. Moss, E.D.W. Mackey, C.D. Son, J. Miwa, et al., Nicotine up-regulates alpha4beta2 nicotinic receptors and ER exit sites via stoichiometry-dependent chaperoning, J. Gen. Physiol. 137 (2011) 59–79.
[20] S. Garcia-Ratés, J. Camarasa, A.I. Sánchez-García, L. Gandía, E. Escubedo, D. Pubill, The effects of 3,4-methylenedioxymethamphetamine (MDMA) on nicotinic receptors: intracellular calcium increase, calpain/caspase 3 activation, and functional upregulation, Toxicol. Appl. Pharmacol. 244 (2010) 344–353.
[21] D. Pubill, S. Garcia-Ratés, J. Camarasa, E. Escubedo, 3,4-Methylenedioxymethamphetamine induces in vivo regional up-regulation of central nicotinic receptors in rats and potentiates the regulatory effects of nicotine on these receptors, Neurotoxicology 35 (2013) 41–49.
[22] J. Camarasa, S.G. Ratés, D. Pubill, E. Escubedo, The involvement of nicotinic receptor subtypes in the locomotor activity and analgesia induced by methamphetamine in mice, Behav. Pharmacol. 20 (2009) 623–630.
[23] J. Camarasa, C. Ros, D. Pubill, E. Escubedo, Tumour necrosis factor alpha suppression by MDMA is mediated by peripheral heteromeric nicotinic receptors, Immunopharmacol. Immunotoxicol. 32 (2010) 265–271.
[24] C. Chipana, J. Camarasa, D. Pubill, E. Escubedo, Memantine prevents MDMA-induced neurotoxicity, Neurotoxicology 29 (2008) 179–183.
[25] C. Chipana, I. Torres, J. Camarasa, D. Pubill, E. Escubedo, Memantine protects against amphetamine derivatives-induced neurotoxic damage in rodents, Neuropharmacology 54 (2008) 1254–1263.
[26] E. Escubedo, J. Camarasa, C. Chipana, S. García-Ratés, D. Pubill, Involvement of nicotinic receptors in methamphetamine- and MDMA-induced neurotoxicity: pharmacological implications, Int. Rev. Neurobiol. 88 (2009) 121–166.
[27] A. Ciudad-Roberts, J. Camarasa, D. Pubill, E. Escubedo, Heteromeric nicotinic receptors are involved in the sensitization and addictive properties of MDMA in mice, Prog. Neuro-psychopharmacol. Biol. Psychiatry 44 (2013) 201–209.
[28] S. Garcia-Ratés, J. Camarasa, E. Escubedo, D. Pubill, Methamphetamine and 3,4-methylenedioxymethamphetamine interact with central nicotinic receptors and induce their up-regulation, Toxicol. Appl. Pharmacol. 223 (2007) 195–205.
[29] K. Matsushima, T. Nagai, S. Kamiyama, Optical isomer analysis of 3,4-methylene-dioxyamphetamine analogues and their stereoselective disposition in rats, J. Anal. Toxicol. 22 (1998) 33–39.
[30] N. Pizarro, J. Ortuño, M. Farré, C. Hernández-López, M. Pujadas, A. Llebaria, et al., Determination of MDMA and its metabolites in blood and urine by gas chromatography-mass spectrometry and analysis of enantiomers by capillary electrophoresis, J. Anal. Toxicol. 26 (2002) 157–165.
[31] T.D. Steele, D.E. Nichols, G.K. Yim, Stereochemical effects of 3,4-methylenedioxymethamphetamine (MDMA) and related amphetamine derivatives on inhibition of uptake of [3H]monoamines into synaptosomes from different regions of rat brain, Biochem. Pharmacol. 36 (1987) 2297–2303.
[32] M.P. Johnson, A.J. Hoffman, D.E. Nichols, Effects of the enantiomers of MDA, MDMA and related analogues on [3H]serotonin and [3H]dopamine release from superfused rat brain slices, Eur. J. Pharmacol. 132 (1986) 269–276.
[33] E. Acquas, A. Pisanu, S. Spiga, A. Plumitallo, G. Zernig, G. Di Chiara, Differential effects of intravenous R,S-(+/-)-3,4-methylenedioxymethamphetamine (MDMA, Ecstasy) and its S(+)- and R(-)-enantiomers on dopamine transmission and extracellular signal regulated kinase phosphorylation (pERK) in the rat nucleus accumbens shell and core, J. Neurochem. 102 (2007) 121–132.
[34] R. Young, R.A. Glennon, MDMA (N-methyl-3,4-methylenedioxyamphetamine) and its stereoisomers: similarities and differences in behavioral effects in an automated activity apparatus in mice, Pharmacol. Biochem. Behav. 88 (2008) 318–331.
[35] M. Ninković, Z. Malicević, V. Selaković, I. Simić, I. Vasiljevi&cacute, N-methyl-3,4-methylenedioxyamphetamine-induced hepatotoxicity in rats: oxidative stress after acute and chronic administration, Vojnosanit. Pregl. Mil.-Med. Pharm. Rev. 61 (2004) 125–131.
[36] S.K. Shenouda, K.C. Lord, E. McIlwain, P.A. Lucchesi, K.J. Varner, Ecstasy produces left ventricular dysfunction and oxidative stress in rats, Cardiovasc. Res. 79 (2008) 662–670.
[37] T.C. Lourenço, G.C. Bósio, N.M. Cassiano, Q.B. Cass, R.L.M. Moreau, Chiral separation of 3,4-methylenedioxymethamphetamine (MDMA) enantiomers using batch chromatography with peak shaving recycling and its effects on oxidative stress status in rat liver, J. Pharm. Biomed. Anal. 73 (2013) 13–17.
[38] C.J. Schmidt, Neurotoxicity of the psychedelic amphetamine, methylenedioxymethamphetamine, J. Pharmacol. Exp. Ther. 240 (1987) 1–7.
[39] L. Frau, N. Simola, A. Plumitallo, M. Morelli, Microglial and astroglial activation by 3,4-methylenedioxymethamphetamine (MDMA) in mice depends on S(+) enantiomer and is associated with an increase in body temperature and motility, J. Neurochem. 124 (2013) 69–78.
[40] P. Huot, T.H. Johnston, K.D. Lewis, J.B. Koprich, M.G. Reyes, S.H. Fox, et al., Characterization of 3,4-methylenedioxymethamphetamine (MDMA) enantiomers in vitro and in the MPTP-lesioned primate: R-MDMA reduces severity of dyskinesia, whereas S-MDMA extends duration of ON-time, J. Neurosci. Off. J. Soc. Neurosci 31 (2011) 7190–7198.
[41] D.E. Nichols, A.J. Hoffman, R.A. Oberlender, P. Jacob, A.T. Shulgin, Derivatives of 1-(1,3-benzodioxol-5-yl)-2-butanamine: representatives of a novel therapeutic class, J. Med. Chem. 29 (1986) 2009–2015.
[42] N. Pizarro, R. de la Torre, M. Farré, J. Segura, A. Llebaria, J. Joglar, Synthesis and capillary electrophoretic analysis of enantiomerically enriched reference standards of MDMA and its main metabolites, Bioorg. Med. Chem. 10 (2002) 1085–1092.
[43] F. Effenberger, J. Jäger, Stereoselective synthesis of (S)-3,4-methylenedioxyamphetamines from (R)-cyanohydrins, Chem. Eur. J. 3 (1997) 1370–1374.
[44] J.M. Wagner, C.J. McElhinny Jr., A.H. Lewin, F.I. Carroll, Stereospecific synthesis of amphetamines, Tetrahedron Asymmetry 14 (2003) 2119–2125.
[45] R. García-Repetto, E. Moreno, T. Soriano, C. Jurado, M.P. Giménez, M. Menéndez, Tissue concentrations of MDMA and its metabolite MDA in three fatal cases of overdose, Forensic Sci. Int. 135 (2003) 110–114.
[46] E.A. Johnson, J.P. O'Callaghan, D.B. Miller, Brain concentrations of d-MDMA are increased after stress, Psychopharmacology (Berl.) 173 (2004) 278–286.
[47] B. Buisson, D. Bertrand, Chronic exposure to nicotine upregulates the human α4β2 nicotinic acetylcholine receptor function, J. Neurosci. 21 (2001) 1819–1829.
[48] K. Brejc, W.J. van Dijk, R.V. Klaassen, M. Schuurmans, J. van Der Oost, A.B. Smit, et al., Crystal structure of an ACh-binding protein reveals the ligand-binding domain of nicotinic receptors, Nature 411 (2001) 269–276.
[49] N. Le Novère, P.-J. Corringer, J.-P. Changeux, The diversity of subunit composition in nAChRs: evolutionary origins, physiologic and pharmacologic consequences, J. Neurobiol. 53 (2002) 447–456.
[50] W.H. Bisson, L. Scapozza, G. Westera, L. Mu, P.A. Schubiger, Ligand selectivity for the acetylcholine binding site of the rat alpha4beta2 and alpha3beta4 nicotinic subtypes investigated by molecular docking, J. Med. Chem. 48 (2005) 5123–5130.
[51] S.B. Hansen, G. Sulzenbacher, T. Huxford, P. Marchot, P. Taylor, Y. Bourne, Structures of Aplysia AChBP complexes with nicotinic agonists and antagonists reveal distinctive binding interfaces and conformations, EMBO J. 24 (2005) 3635–3646.
[52] S.-X. Li, S. Huang, N. Bren, K. Noridomi, C.D. Dellisanti, S.M. Sine, et al., Ligand-binding domain of an α7-nicotinic receptor chimera and its complex with agonist, Nat. Neurosci. 14 (2011) 1253–1259.
[53] X. Xiu, N.L. Puskar, J.A.P. Shanata, H.A. Lester, D.A. Dougherty, Nicotine binding to brain receptors requires a strong cation-pi interaction, Nature 458 (2009) 534–537.
[54] D.C. Kombo, T.A. Hauser, V.P. Grinevich, M.S. Melvin, J.-P. Strachan, S.S. Sidach, et al., Pharmacological properties and predicted binding mode of arylmethylene quinuclidine-like derivatives at the α3β4 nicotinic acetylcholine receptor (nAChR), Bioorg. Med. Chem. Lett. 23 (2013) 1450–1455.
[55] T. Takahashi, H. Yamashita, S. Nakamura, H. Ishiguro, T. Nagatsu, H. Kawakami, Effects of nerve growth factor and nicotine on the expression of

nicotinic acetylcholine receptor subunits in PC12 cells, Neurosci. Res. 35 (1999) 175–181.
[56] Y.C. Cheng, W.H. Prusoff, Mouse ascites sarcoma 180 thymidylate kinase. General properties, kinetic analysis, and inhibition studies, Biochemistry (Mosc.) 12 (1973) 2612–2619.
[57] Y. Xiao, K.J. Kellar, The comparative pharmacology and up-regulation of rat neuronal nicotinic receptor subtype binding sites stably expressed in transfected mammalian cells, J. Pharmacol. Exp. Ther. 310 (2004) 98–107.
[58] D.A. Case, T.A. Darden, T.E. Cheatham III, C.L. Simmerling, J. Wang, R.E. Duke, et al., AMBER 9, Univ. Calif. San Franc., 2006.
[59] V. Hornak, R. Abel, A. Okur, B. Strockbine, A. Roitberg, C. Simmerling, Comparison of multiple Amber force fields and development of improved protein backbone parameters, Proteins 65 (2006) 712–725.
[60] J. Wang, R.M. Wolf, J.W. Caldwell, P.A. Kollman, D.A. Case, Development and testing of a general amber force field, J. Comput. Chem. 25 (2004) 1157–1174.
[61] C.I. Bayly, P. Cieplak, W. Cornell, P.A. Kollman, A well-behaved electrostatic potential based method using charge restraints for deriving atomic charges: the RESP model, J. Phys. Chem. 97 (1993) 10269–10280.
[62] M.J. Frisch, G.W. Trucks, H.B. Schlegel, G.E. Scuseria, M.A. Robb, J.R. Cheeseman, et al., Gaussian 03, Revision B. 01, Gaussian, Inc, Pittsburgh, PA, USA, 2003.
[63] W.L. Jorgensen, J. Chandrasekhar, J.D. Madura, R.W. Impey, M.L. Klein, Comparison of simple potential functions for simulating liquid water, J. Chem. Phys. 79 (1983) 926.
[64] Q. Cui, T. Sulea, J.D. Schrag, C. Munger, M.-N. Hung, M. Naïm, et al., Molecular dynamics-solvated interaction energy studies of protein-protein interactions: the MP1-p14 scaffolding complex, J. Mol. Biol. 379 (2008) 787–802.
[65] M. Naïm, S. Bhat, K.N. Rankin, S. Dennis, S.F. Chowdhury, I. Siddiqi, et al., Solvated interaction energy (SIE) for scoring protein-ligand binding affinities. 1. Exploring the parameter space, J. Chem. Inf. Model. 47 (2007) 122–133.
[66] S.F. Boys, F. Bernardi, The calculation of small molecular interactions by the differences of separate total energies. Some procedures with reduced errors, Mol. Phys. 19 (1970) 553–566.
[67] V.S. Bryantsev, M.S. Diallo, W.A. Goddard III, Calculation of solvation free energies of charged solutes using mixed cluster/continuum models, J. Phys. Chem. B 112 (2008) 9709–9719.